

Experimental and Theoretical Investigations of the Stability, Energetics, and Structures of H_2PO_4^- , $\text{H}_2\text{P}_2\text{O}_7^{2-}$, and $\text{H}_3\text{P}_3\text{O}_{10}^{2-}$ in the Gas Phase

Xue-Bin Wang,^{†,‡} Erich R. Vorpagel,[§] Xin Yang,^{†,‡} and Lai-Sheng Wang^{*,†,‡}

Department of Physics, Washington State University, 2710 University Drive, Richland, Washington 99352, W. R. Wiley Environmental Molecular Sciences Laboratory, Pacific Northwest National Laboratory, MS K8-88, P.O. Box 999, Richland, Washington 99352, and MSCF Visualization and User Services Group, W. R. Wiley Environmental Molecular Sciences Laboratory, Pacific Northwest National Laboratory, MS K8-91, P.O. Box 999, Richland, Washington 99352

Received: August 20, 2001; In Final Form: September 18, 2001

The stability, energetics, and structures of three common inorganic phosphate species, H_2PO_4^- , $\text{H}_2\text{P}_2\text{O}_7^{2-}$, $\text{H}_3\text{P}_3\text{O}_{10}^{2-}$, and their corresponding neutral radical and monoanions, were investigated in the gas phase using photodetachment photoelectron spectroscopy and theoretical calculations. We found that $\text{H}_2\text{P}_2\text{O}_7^{2-}$ and $\text{H}_3\text{P}_3\text{O}_{10}^{2-}$ are stable in the gas phase with adiabatic electron binding energies of 1.16 and 2.45 eV, respectively. A very high adiabatic electron binding energy of 4.57 eV was measured for H_2PO_4^- . The intramolecular Coulomb repulsion energies in $\text{H}_2\text{P}_2\text{O}_7^{2-}$ (~ 2.7 eV) and $\text{H}_3\text{P}_3\text{O}_{10}^{2-}$ (~ 2.3 eV) were estimated from photon-energy-dependent photoelectron spectra. Density-functional theory calculations were used to search the optimal geometries for both the doubly and singly charged species. We found only one minimum energy conformation for $\text{H}_2\text{P}_2\text{O}_7^{2-}$ with two intramolecular H-bonds and C_2 symmetry and three minimum energy structures for $\text{H}_3\text{P}_3\text{O}_{10}^{2-}$. The lowest energy structure of $\text{H}_3\text{P}_3\text{O}_{10}^{2-}$ has three intramolecular H-bonds that do not share a common oxygen atom. The calculated electron detachment energy of H_2PO_4^- agrees with the experimental value well, but the calculated detachment energies for $\text{H}_2\text{P}_2\text{O}_7^{2-}$ and $\text{H}_3\text{P}_3\text{O}_{10}^{2-}$ are ~ 0.3 and ~ 0.7 eV smaller than the experimental values, respectively. The observed spectral features, due to removal of electrons from lone-pair oxygen orbitals in the phosphate groups, were assigned qualitatively on the basis of the theoretical calculations.

1. Introduction

The pyrophosphate linkage P–O–P plays an essential role in biochemistry and is the main structural form through which energy is transmitted within living cells.^{1,2} In the physiological pH range pyrophosphate and adenosine triphosphate (ATP) have two to three negative charges. The Coulomb repulsion between the excess charges at least partly renders pyrophosphate and ATP as “energy-rich” molecules. There have been several theoretical studies on the hydrolysis of pyrophosphate in the gas phase.^{3–6} The structure of pyrophosphate and its dependence upon the excess charges were found to be crucial in understanding the mechanism and thermodynamic properties of the phosphoryl transfer reactions in biological systems. One central issue in all of these calculations is whether the multiply charged pyrophosphate anions are intrinsically stable. Experimental gas phase study of the isolated anionic phosphate species is valuable in terms of obtaining intrinsic structures and energetic information and providing benchmarks for theoretical calculations. Yet, there is little experimental information of the anionic phosphates in the gas phase. Only free energies of hydration of the anionic phosphates have been measured.⁷ The electron binding energy of the simplest dihydrogen phosphate anion (H_2PO_4^-) has not

been measured directly. The stability of isolated multiply charged phosphate species is also unknown.

We have developed an experimental technique to study gaseous multiply charged anions (MCAs) using photodetachment photoelectron spectroscopy (PES) and electrospray ionization.⁸ PES is ideal for probing the intrinsic properties of free MCAs and directly yields information about their stability, intramolecular Coulomb repulsion, and solvation effects. We were able to observe directly the repulsive Coulomb barrier (RCB) present universally in MCAs and estimate its magnitude by measuring PES spectra at different photon energies.⁹ More importantly, we found that the RCB is equal in magnitude to the Coulomb repulsion between the excess charges at the equilibrium structure of an MCA, hence providing us a unique way to experimentally determine the electrostatic energy stored in an MCA.^{10,11} This experimental technique is ideal for the investigation of the pyrophosphate MCAs in the gas phase.

We obtained previously a PES spectrum of PO_3^- ,¹² an important intermediate involved in phosphoryl transfer reactions. In the current paper, we report a combined experimental and theoretical investigation on the dihydrogen phosphate anion (H_2PO_4^-) and two common pyrophosphate dianions, $\text{H}_2\text{P}_2\text{O}_7^{2-}$ and $\text{H}_3\text{P}_3\text{O}_{10}^{2-}$, as well as the corresponding neutral and singly charged species. Specifically, we were interested in obtaining their electron binding energies, their stability and structures, and the intramolecular Coulomb repulsion in the dianions.

2. Experimental Method

The experiments were carried out with a PES facility that involves a magnetic-bottle time-of-flight photoelectron analyzer

* Corresponding author. E-mail: ls.wang@pnl.gov.

[†] Washington State University.

[‡] W. R. Wiley Environmental Molecular Sciences Laboratory, Pacific Northwest National Laboratory.

[§] MSCF Visualization and User Services Group, W. R. Wiley Environmental Molecular Sciences Laboratory, Pacific Northwest National Laboratory.

and an electrospray ion source. Details of the apparatus have been published previously¹³ and only a brief description is given here. To produce the desired anionic species, we used a 5×10^{-4} molar solution of the corresponding sodium salts (Na_3PO_4 , $\text{Na}_4\text{P}_2\text{O}_7$, and $\text{Na}_5\text{P}_3\text{O}_{10}$) in a water/methanol mixed solvent (10/90 volume ratio). Each solution was sprayed through a 0.01 mm diameter syringe needle at ambient atmosphere and at a high voltage bias of -2.2 kV, producing highly charged liquid droplets, which were fed into a desolvation capillary. Negatively charged molecular ions emerging from the desolvation capillary were guided by a radio frequency-only quadrupole ion guide into a 3-D quadrupole ion trap, where the ions were accumulated for 0.1 s before being pushed into the extraction zone of a time-of-flight mass spectrometer. The major anions are H_2PO_4^- , $\text{H}_2\text{P}_2\text{O}_7^{2-}$, and $\text{H}_3\text{P}_3\text{O}_{10}^{2-}$. Anions with higher charges, such as HPO_4^{2-} , PO_4^{3-} , $\text{HP}_2\text{O}_7^{3-}$, $\text{P}_2\text{O}_7^{4-}$, $\text{H}_2\text{P}_3\text{O}_{10}^{3-}$, $\text{HP}_3\text{O}_{10}^{4-}$, and $\text{P}_3\text{O}_{10}^{5-}$, which we were also interested, were not observed, presumably due to their instability as a result of the strong intramolecular Coulomb repulsion.

In the PES experiment, the anions of interest were mass selected and decelerated before being intercepted by a laser beam in the detachment zone of the magnetic-bottle photoelectron analyzer. Both a Nd:YAG laser (266 nm) and an excimer laser (193 and 157 nm) were used for photodetachment. Photoelectron time-of-flight spectra were collected at nearly 100% efficiency by the magnetic bottle and converted to kinetic energy spectra, calibrated by the known spectra of I^- and O^- . The electron kinetic energy resolution was $\Delta E/E \sim 2\%$, i.e., 20 meV for 1 eV electrons. Binding energy spectra were obtained by subtracting the kinetic energy spectra from the photon energy.

3. Theoretical Method

The NWChem computational chemistry program¹⁴ was used to determine the geometrical and electronic structures of H_2PO_4^- , $\text{H}_2\text{P}_2\text{O}_7^{2-}$, and $\text{H}_3\text{P}_3\text{O}_{10}^{2-}$. All species were optimized using density functional theory (DFT)^{15,16} and the hybrid B3LYP exchange-correlation functional.^{17,18} We used the TZVP+ basis set, which was derived from the DFT-optimized TZVP basis set¹⁹ by adding diffuse functions derived from an even-tempered expansion of the outermost functions in the original basis set. An additional diffuse s function was added to each hydrogen atom (exponent = 0.04573), and diffuse s and p functions were added to oxygen and phosphorus atoms (exponents 0.08142 and 0.04812 on O, 0.04026 and 0.02813 on P). Frequencies were calculated for all species to confirm the geometries were minima on the potential energy surface. Single-point MP2 energies were calculated using the optimized DFT structures and the Dunning-Hay-DZP+Rydberg basis set.²⁰ The Extensible Computational Chemistry Environment (Ecce)²¹ was used to setup, launch, and evaluate the results from NWChem. Conformational energy differences reported are those from the DFT-optimized calculations. We define the vertical electron detachment energy (VDE) of a dianion as the difference in total energy between the optimized dianion complex and the singly charged anion calculated at the dianion geometry. We define the adiabatic electron detachment energy (ADE) of a dianion as the difference in energy between the optimized geometries of the dianion and singly charged anion complexes. The VDE and ADE of a singly charged anion are defined in a similar way between the anion and the corresponding neutral.

4. Experimental Results

The PES spectra of H_2PO_4^- are shown in Figure 1 at 193 and 157 nm. Two relatively broad features centered at 5.0 (X)

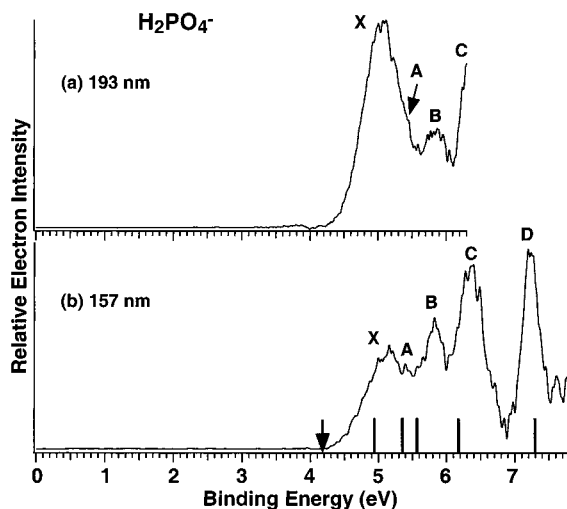


Figure 1. Photoelectron spectra of H_2PO_4^- at (a) 193 nm (6.424 eV) and (b) 157 nm (7.866 eV). The calculated ADE (arrow) and VDEs (vertical bars) are indicated.

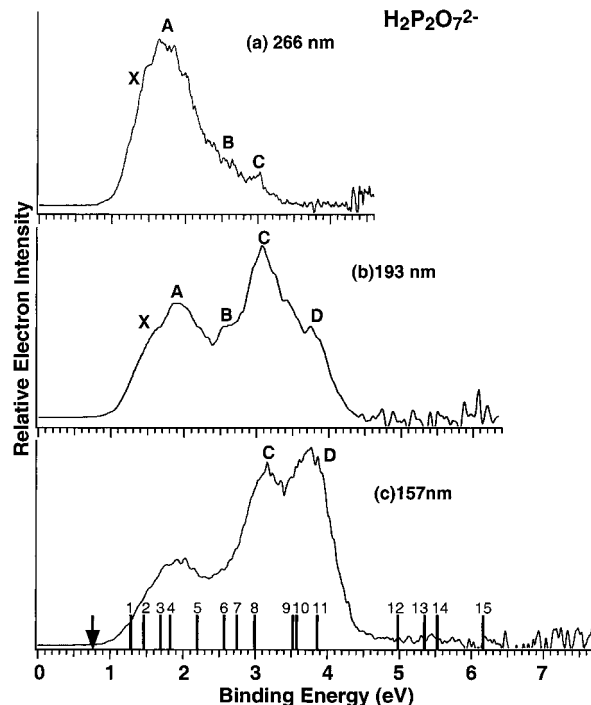


Figure 2. Photoelectron spectra of $\text{H}_2\text{P}_2\text{O}_7^{2-}$ at (a) 266 nm (4.661 eV), (b) 193 nm, and (c) 157 nm. The calculated ADE (arrow) and VDEs (vertical bars) are indicated.

and 5.8 eV (B) were resolved in the 193-nm spectrum. The onset of a third peak (C) was observed as a tail at 6.3 eV. At 157 nm (Figure 1b), the C peak and a new feature D at 7.25 eV appeared dominantly. One small feature (A) was resolved between the X and B peaks in the 157 nm spectrum. Close examination of the 193 nm spectrum indicates that the feature A was superimposed as a shoulder on the much stronger X peak. The intensity of the X band was observed to decrease significantly at 157 nm.

Figure 2 shows the PES spectra of $\text{H}_2\text{P}_2\text{O}_7^{2-}$ at three photon energies. Five broad features (X and A–D) were discernible in the 193 nm spectrum (Figure 1b), whereas no new features were observed at 157 nm (Figure 1c). At 266 nm (Figure 1a), only the X and A bands showed up as dominant features, and the intensities of the B and C bands greatly decreased. The peak D completely disappeared at 266 nm, due to the RCB, as will be

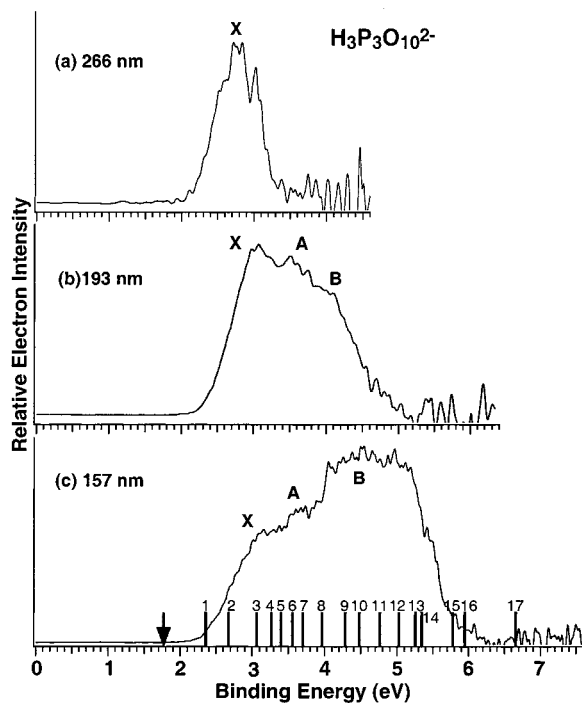


Figure 3. Photoelectron spectra of $\text{H}_3\text{P}_3\text{O}_{10}^{2-}$ at (a) 266 nm, (b) 193 nm, and (c) 157 nm. The calculated ADE (arrow) and VDEs (vertical bars) are indicated.

discussed later. The intensity of the D feature also decreased from the 157 to 193 nm spectra, again due to the RCB. From the photon-energy-dependent PES spectra, we will estimate later the RCB height and hence the intramolecular Coulomb repulsion.

The spectra of $\text{H}_3\text{P}_3\text{O}_{10}^{2-}$ are shown in Figure 3 at three photon energies. These spectra are very broad and congested due to the large size of $\text{H}_3\text{P}_3\text{O}_{10}^{2-}$. The 193 nm spectrum of $\text{H}_3\text{P}_3\text{O}_{10}^{2-}$ (Figure 3b) showed three overlapping features (X, A, and B). At 266 nm, the A and B bands were completely cut off, and the detachment cross section of the X band was greatly reduced. The X band also shifted to lower binding energy compared to that at 193 nm. At 157 nm, more congested features were observed. The photon energy dependence of the $\text{H}_3\text{P}_3\text{O}_{10}^{2-}$ spectra was also due to the RCB and will be discussed later.

The PES features of H_2PO_4^- (Figure 1) were relatively sharp compared to that of $\text{H}_2\text{P}_2\text{O}_7^{2-}$ and $\text{H}_3\text{P}_3\text{O}_{10}^{2-}$. The ADEs for each species were measured by drawing a straight line at the leading edge of the respective X bands and then adding a constant to the intercept with the binding energy axis to take into account both the instrumental resolution and a finite thermal effect. The VDEs were obtained from the PES band maxima for all observed transitions. Due to the broad nature of the spectra, only estimates of the ADEs and VDEs could be obtained. Table 1 lists the measured ADEs and VDEs for the ground-state transitions of H_2PO_4^- , $\text{H}_2\text{P}_2\text{O}_7^{2-}$, and $\text{H}_3\text{P}_3\text{O}_{10}^{2-}$. The ADEs for the ground-state transitions also represent the adiabatic electron affinities for the corresponding neutral (H_2PO_4) and monoanions ($\text{H}_2\text{P}_2\text{O}_7^-$ and $\text{H}_3\text{P}_3\text{O}_{10}^-$). The VDEs of all the observed PES features for each species are given in Table 2 and compared with the theoretical results.

5. Computational Results

5.1. $\text{H}_2\text{PO}_4^-/\text{H}_2\text{PO}_4$. Two minimum energy conformations were found for H_2PO_4^- . The global minimum has C_2 symmetry with the O–H bonds pointing away from each other forming a

TABLE 1: Experimental and Theoretical Adiabatic (ADE) and Vertical (VDE) Detachment Energies for the Ground State Transitions of HPO_4^- , $\text{H}_2\text{P}_2\text{O}_7^{2-}$, and $\text{H}_3\text{P}_3\text{O}_{10}^{2-}$ (eV)^a

	ADE ^b		VDE	
	exp	theo	exp	theo
H_2PO_4^-	4.57(10)	4.16	5.06(5)	4.92
$\text{H}_2\text{P}_2\text{O}_7^{2-}$	1.16(10)	0.72	1.59(10)	1.26
$\text{H}_3\text{P}_3\text{O}_{10}^{2-}$	2.45(10)	1.73	3.06(10)	2.32

^a The numbers in the parentheses represent the uncertainties in the last digit. The VDE was measured from the peak maximum. ^b Adiabatic electron affinities of the corresponding species with one less charge.

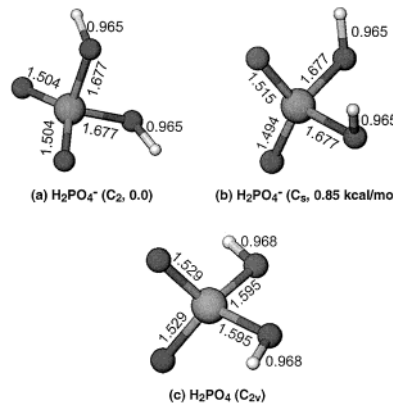


Figure 4. Optimized structures for the global minimum (a) and a low-lying isomer (b) of H_2PO_4^- and the global minimum (c) of the H_2PO_4 neutral.

TABLE 2: Experimental Vertical Detachment Energies, Compared to Theoretical Orbital Ionization Potentials (IPs) (eV) for the Valence Orbitals of H_2PO_4^- , $\text{H}_2\text{P}_2\text{O}_7^{2-}$, and $\text{H}_3\text{P}_3\text{O}_{10}^{2-}$ at the Combined B3LYP/TZVP+ and SCF/DZP+Rydberg Levels of Theory

	H_2PO_4^-		$\text{H}_2\text{P}_2\text{O}_7^{2-}$		$\text{H}_3\text{P}_3\text{O}_{10}^{2-}$	
	exp	theo	exp	theo	exp	theo
IP1	5.06 (X)	4.92	1.59 (X)	1.26	3.06 (X)	2.32
IP2	5.42 (A)	5.34				
IP3	5.82 (B)	5.58	1.90 (A)	1.68		
IP4	6.37 (C)	6.18			1.80	3.56 (A)
IP5	7.27 (D)	7.31	2.56 (B)	2.19		
IP6		8.22		2.55		
IP7			~3.1 (C)	2.72		
IP8				2.99	4~6 (B)	3.94
IP9				~3.8 (D)	3.52	
IP10					3.56	
IP11					3.83	
IP12					4.96	
IP13					5.35	
IP14					5.51	
IP15					6.19	
IP16						5.95
IP17						6.68

torsion angle with a nonprotonated oxygen atom of about 18.6 degrees, as shown in Figure 4a. The C_s symmetry conformation with the O–H bonds lining up with the same nonprotonated oxygen atom (torsion angle of 11.5°) was higher in energy by 0.85 kcal/mol (Figure 4b). These conformations are different from the C_{2v} symmetry (similar to Figure 4c) obtained previously using the 6-31G* basis set at the Hartree–Fock level of theory.²² The C_{2v} structure was found not to be a minimum in the current study.

To estimate the theoretical ADEs, the minimized structures for the corresponding neutral H_2PO_4 must be found. The ground state of this radical is open shell with an unpaired electron. Starting from the minimum energy conformations, we removed

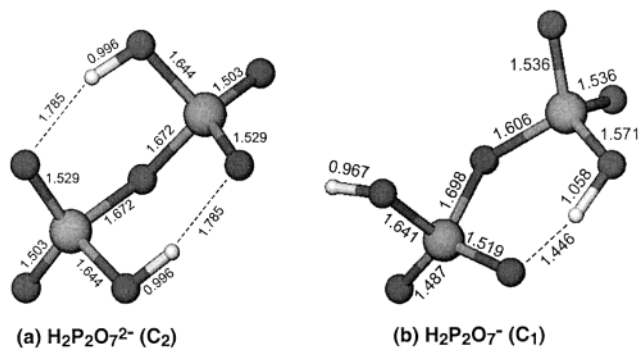


Figure 5. Optimized structures for (a) $\text{H}_2\text{P}_2\text{O}_7^{2-}$ and (b) $\text{H}_2\text{P}_2\text{O}_7^-$.

one electron from the highest occupied molecular orbital (HOMO) of H_2PO_4^- and performed a geometry optimization using unrestricted DFT calculations on the doublet species. Only one minimum energy conformation (with C_{2v} symmetry) was found for the neutral dihydrogen phosphate as shown in Figure 4c.

5.2. $\text{H}_2\text{P}_2\text{O}_7^{2-}/\text{H}_2\text{P}_2\text{O}_7^-$. Exploration of the potential energy surface for $\text{H}_2\text{P}_2\text{O}_7^{2-}$ revealed only one minimum energy conformation having two intramolecular H-bonds (1.785 Å) and C₂ symmetry. The structure is shown in Figure 5a and is similar to previous calculations at other levels of theory and basis sets.^{3–6} Figure 5b shows the structure of the $\text{H}_2\text{P}_2\text{O}_7^-$ monoanion. One of the terminal hydrogen atoms rotates away, breaking a H-bond and the symmetry, while the other H-bond becomes much stronger (1.446 Å). This is consistent with removal of an electron from the symmetric HOMO of the dianion followed by rearrangement of the electron density giving the oxygen atom with the H-bond the greatest negative charge (section 5.5). Note also the difference in bond length between the P and O atoms in the two structures. For the symmetric dianion, a bond length of 1.503 Å is observed for the two terminal bonds. For the monoanion, one bond has shortened to 1.487 Å while the other

has lengthened to 1.536 Å. The latter also contains less electron density (according to Mulliken population analysis) and most of the spin density.

5.3. $\text{H}_3\text{P}_3\text{O}_{10}^{2-}/\text{H}_3\text{P}_3\text{O}_{10}^-$. Three minimum energy structures were found for $\text{H}_3\text{P}_3\text{O}_{10}^{2-}$, as shown in Figure 6a-c. Structure (a) is the global energy minimum having three intramolecular H-bonds (1.447, 1.711, and 1.829 Å) that do not share a common oxygen atom. The two local minima both have H-bonds that share a common oxygen atom from the center phosphate. Structure (b) is 7.8 kcal/mol higher in energy and has features similar to $\text{H}_2\text{P}_2\text{O}_7^{2-}$ on one end. It has three H-bonds (1.651, 1.930, and 2.032 Å), two of which share a common oxygen atom from the center phosphate. Structure (c) is 11.9 kcal/mol higher in energy than structure (a). It also has three intramolecular H-bonds: one of the central phosphate oxygen atoms forms a bifurcated H-bond with two hydrogen atoms on one terminal phosphate group (1.823, 2.031 Å), while another central phosphate oxygen atom forms a single H-bond with a hydrogen atom on the other terminal phosphate group (1.875 Å).

Two minimum energy conformations were found for the $\text{H}_3\text{P}_3\text{O}_{10}^-$ monoanion, as shown in Figure 6d,e. Three intramolecular H-bonds are present in both conformations, 1.573, 1.768, and 1.952 Å for (d) and 1.533, 1.966, and 2.169 Å for (e). The global minimum (d) is similar to structure (a) while structure (e) is similar to structure (c). The energy difference between the two monoanions is only 0.89 kcal/mol. Again the P–O bond whose oxygen atom contains most of the spin density is the one that lengthens, from 1.495 Å in structure (a) to 1.534 Å in structure (d). This also corresponds to the region of the molecule where the HOMO is located (see below) from whence the electron was removed.

5.4. Electron Binding Energies. There are significant structural changes between H_2PO_4^- and H_2PO_4 and between the dianions and the monoanions for the di- and triphosphate, consistent with the broad bands observed in the PES spectra. Calculated ADEs and VDEs for the ground-state transitions are

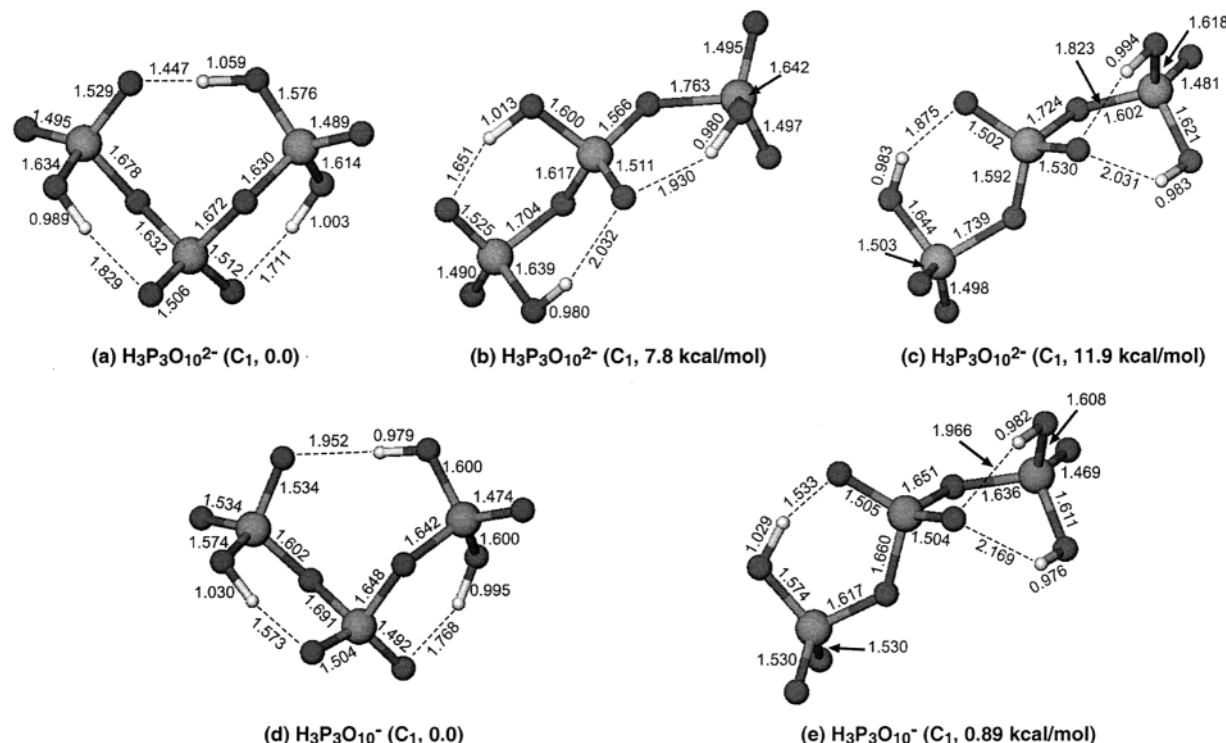


Figure 6. Optimized structures for the global minimum (a) and two local minima (b) and (c) of $\text{H}_3\text{P}_3\text{O}_{10}^{2-}$, and the global minimum (d) and a local

TABLE 3: Calculated Adiabatic and Vertical Detachment Energies for the Ground State Transitions for the Low-Lying Isomers of H_2PO_4^- , $\text{H}_2\text{P}_2\text{O}_7^{2-}$, and $\text{H}_3\text{P}_3\text{O}_{10}^{2-}$ (B3LYP/TZVP+)

	ADE (eV)	VDE (eV)
$\text{H}_2\text{PO}_4^- C_2$	4.16	4.92
$\text{H}_2\text{PO}_4^- C_s$	4.13	4.94
$\text{H}_2\text{P}_2\text{O}_7^{2-}$	0.72	1.26
$\text{H}_3\text{P}_3\text{O}_{10}^{2-}$ (a)	1.73	2.32
$\text{H}_3\text{P}_3\text{O}_{10}^{2-}$ (b)	1.43	2.32
$\text{H}_3\text{P}_3\text{O}_{10}^{2-}$ (c)	1.25	2.15

TABLE 4: Molecular Orbital Energies (Hartrees and eV) for the LUMO and the First Seventeen Highest Energy Occupied Orbitals at the SCF/DZP+Rydberg Level of Theory

	H_2PO_4^-		$\text{H}_2\text{P}_2\text{O}_7^{2-}$		$\text{H}_3\text{P}_3\text{O}_{10}^{2-}$	
	Hartree	eV	Hartree	eV	Hartree	eV
LUMO	0.0816	2.220	0.1366	3.717	0.1299	3.535
HOMO	-0.2447	-6.658	-0.1304	-3.548	-0.1752	-4.767
HOMO-1	-0.2601	-7.077	-0.1363	-3.709	-0.1877	-5.107
HOMO-2	-0.2691	-7.322	-0.1460	-3.973	-0.2017	-5.488
HOMO-3	-0.2911	-7.921	-0.1504	-4.092	-0.2094	-5.698
HOMO-4	-0.3329	-9.058	-0.1645	-4.476	-0.2143	-5.831
HOMO-5	-0.3591	-9.771	-0.1779	-4.841	-0.2194	-5.970
HOMO-6	-0.3659	-9.956	-0.1840	-5.007	-0.2257	-6.141
HOMO-7	-0.4242	-11.54	-0.1939	-5.276	-0.2348	-6.389
HOMO-8	-0.4476	-12.18	-0.2136	-5.812	-0.2472	-6.726
HOMO-9	-0.4645	-12.64	-0.2148	-5.845	-0.2544	-6.922
HOMO-10	-0.5393	-14.67	-0.2247	-6.114	-0.2645	-7.197
HOMO-11	-0.6101	-16.60	-0.2664	-7.249	-0.2742	-7.461
HOMO-12	-1.0723	-29.18	-0.2806	-7.635	-0.2773	-7.545
HOMO-13	-1.1027	-30.00	-0.2867	-7.801	-0.2863	-7.790
HOMO-14	-1.2262	-33.36	-0.3116	-8.479	-0.2899	-7.888
HOMO-15	-5.3105	-144.5	-0.3364	-9.153	-0.3059	-8.324
HOMO-16	-5.3113	-144.5	-0.3393	-9.232	-0.3121	-8.492

given in Table 1, and Table 3 for different isomers. Since structures (b) and (c) are much higher in energy than structure (a) for the triphosphate dianion, very little is expected to be present under the conditions of the current experiment.

Molecular orbital energies for the global minima of H_2PO_4^- , $\text{H}_2\text{P}_2\text{O}_7^{2-}$, and $\text{H}_3\text{P}_3\text{O}_{10}^{2-}$ calculated using the SCF/DZP+Rydberg level of theory (B3LYP/TZVP+ optimized structures) are given in Table 4. All anions have occupied orbitals with negative energies, consistent with their being stable in the gas phase. Also note their relative energies are consistent with the observed experimental detachment energies. Using the VDEs calculated from the B3LYP/TZVP+ energies in Table 1 for the ground-state transitions, one can estimate the VDEs by removing electrons from deeper MOs using the relative energy differences given in Table 4. These relative orbital ionization potentials (IPs) for removing electrons from different MOs, are shown in Table 2 and compared with the experimental results.

5.5. Molecular Orbitals. The first five occupied MOs for H_2PO_4^- are shown in Figure 7. All of these MOs are dominated by lone pairs on the oxygen atoms. The HOMOs for the global minimum conformations of $\text{H}_2\text{P}_2\text{O}_7^{2-}$ and $\text{H}_3\text{P}_3\text{O}_{10}^{2-}$ are shown in Figure 8. Removal of an electron from the HOMO of the three anions is consistent with the structural changes seen in the resulting doublet species: reduced electron density weakens internal hydrogen bonds, causing torsional changes.

6. Discussion

6.1. Repulsive Coulomb Barrier and Intramolecular Coulomb Repulsion in the Doubly-Charged Anions. As shown before,^{8,23} there exists a RCB against electron detachment in MCAs because the final products consist of two negatively

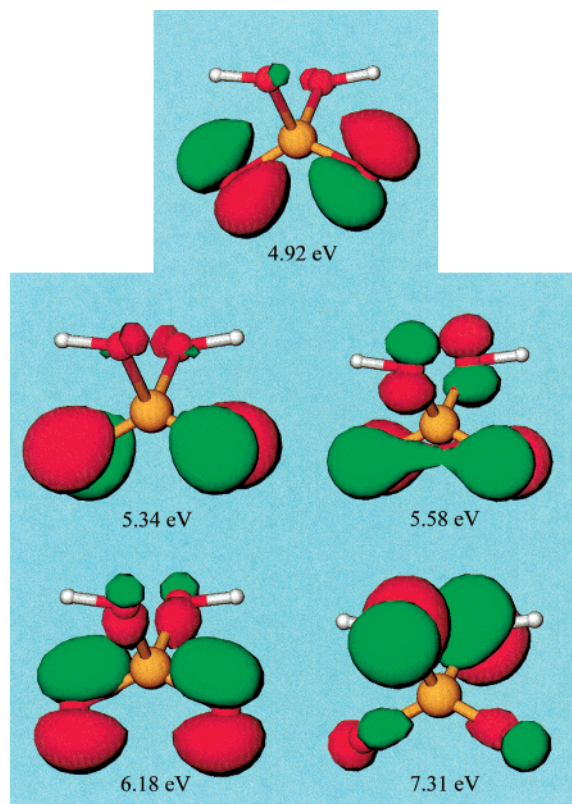


Figure 7. Molecular orbitals (0.069 iso-surface) and calculated ionization potentials of the five highest occupied orbitals for H_2PO_4^- from DZP+Rydberg SCF calculations.

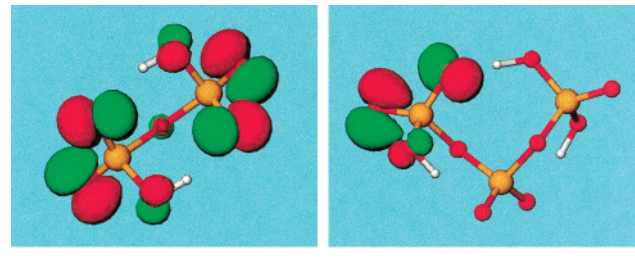


Figure 8. Highest occupied molecular orbitals for (a) $\text{H}_2\text{P}_2\text{O}_7^{2-}$ and (b) $\text{H}_3\text{P}_3\text{O}_{10}^{2-}$.

charged particles and their long-range interaction is primarily the Coulomb repulsion. We can estimate the RCB from PES spectra of an MCA through photon-energy-dependent studies, as qualitatively illustrated in Figure 9. For example, if the photon energy $h\nu_1$ is below the RCB, there will be either no PES signal or reduced PES signal (due to electron tunneling). In the tunneling regime, the normal Franck–Condon envelopes are modified by the tunneling probability for different vibrational levels, often resulting in PES bands shifted to lower electron binding energies (EB).²⁴ At this photon energy, the RCB can be estimated to be greater than $(h\nu_1 - \text{EB})$. On the other hand, the photon energy $h\nu_3$ is above the RCB, and in this case the RCB would be estimated to be less than $(h\nu_3 - \text{EB})$. Hence, we can bracket the RCB: $(h\nu_1 - \text{EB}) < \text{RCB} < (h\nu_3 - \text{EB})$. If we find a photon energy $(h\nu_2)$ to be near the top of the RCB, we obtain $\text{RCB} \sim (h\nu_2 - \text{EB})$.

The significantly decreased intensity of the D feature ($\text{EB} \sim 3.8$ eV) of $\text{H}_2\text{P}_2\text{O}_7^{2-}$ in the 193 nm spectrum (Figure 2b) is due to the RCB, indicating that the 193 nm photon is lower than the RCB of this detachment channel, i.e., $\text{RCB} > 2.6$ eV (6.4–3.8). On the other hand, the strong electron signal of the

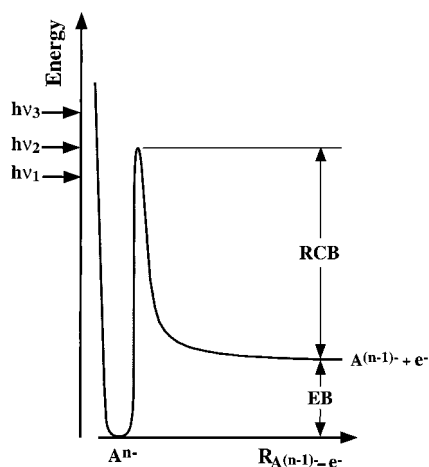


Figure 9. Schematic potential energy curve showing the asymptotic binding energy (EB) and the repulsive Coulomb barrier (RCB) for a multiply charged anion, A^{n-} , and how photon-energy-dependent detachment spectra can be used to estimate the RCB.

A feature (EB \sim 1.8 eV) at the 266 nm spectrum suggests that RCB $<$ 2.8 eV (4.6–1.8). Therefore, we estimated the RCB in $H_2P_2O_7^{2-}$ to be \sim 2.7 eV.

For $H_3P_3O_{10}^{2-}$, the very weak signal and the shift to lower binding energy of the 266 nm spectrum (Figure 3a) suggested that the 266 nm is below the RCB for the ground-state transition (ADE = 2.45 eV). Thus the RCB is $>$ 2.2 eV. From the cutoff at 193 and 157 nm spectra, we estimated the RCB in $H_3P_3O_{10}^{2-}$ to be \sim 2.3 eV. Hence we determined approximately the intramolecular Coulomb repulsion in $H_2P_2O_7^{2-}$ and $H_3P_3O_{10}^{2-}$ to be 2.7 and 2.3 eV, respectively.

We have shown previously^{8–12} that the RCB is equal in magnitude to the intramolecular Coulomb repulsion among the excess charges in a MCA. For a dianion, the intramolecular Coulomb repulsion can be estimated simply according to Coulomb's law, $e^2/4\pi\epsilon_0 r$, or $14.4/r$ in electronvolts, where r is the effective distance between the two excess charges in Å. The two excess charges in $H_2P_2O_7^{2-}$ and $H_3P_3O_{10}^{2-}$ are distributed among the oxygen atoms of the phosphate groups, making it difficult to pin down their locations. From Mulliken population analyses, we noted that the two terminal, non-H-bonded oxygen atoms in the ground-state structures of each dianion carry the most negative charge. If we make a simple assumption and use the distances between these oxygen atoms, 5.18 Å for $H_2P_2O_7^{2-}$ (Figure 5a) and 6.79 Å for $H_3P_3O_{10}^{2-}$ (Figure 6a), we obtained Coulomb repulsion energies of 2.78 and 2.12 eV for $H_2P_2O_7^{2-}$ and $H_3P_3O_{10}^{2-}$, respectively. These estimates are consistent with the experimentally determined RCB values of \sim 2.7 and \sim 2.3 eV for $H_2P_2O_7^{2-}$ and $H_3P_3O_{10}^{2-}$, respectively.

6.2. Comparison of Experimental and Theoretical Results. The PES features shown in Figures 1–3 represent transitions from the ground state of the anion (dianions) to the ground and excited states of the corresponding neutral (singly charged anions). Within the single-particle approximation (Koopmans' theorem), these PES features can be viewed as removing electrons from the occupied molecular orbitals of the ground states of the anions.

Our calculations indicated that the first five occupied MOs of $H_2PO_4^-$ consist purely of the oxygen lone-pair orbitals (Figure 7). Removal of an electron from each of these MOs gives rise to the five features (X and A–D) in Figure 1. The calculated VDEs are compared with the experimental values in Table 2 and are shown in Figure 1 as vertical bars. Excellent agreement between the calculated VDEs and the experimental values was

found. The calculated VDEs are also in good agreement with a previous calculation.²⁵ The calculated ADE (listed in Table 1 and shown in Figure 1 as an arrow), however, was smaller than the experimental value by \sim 0.4 eV. The calculated ADE and VDE for the C_s symmetry isomer are almost the same as for the C_2 structure (Table 3). Because the C_s structure is only 0.85 kcal/mol higher in total energy, it is likely that both the C_2 and C_s isomers were present in our experiment at room temperature.

The valence MOs of $H_2P_2O_7^{2-}$ are also constructed mostly from the oxygen lone-pair p orbitals. The HOMO is shown in Figure 8a. The calculated ADE and VDE for the ground-state transition (Table 1) are \sim 0.3 eV less than the corresponding experimental values. The calculated VDEs or the orbital IPs for the valence electrons are listed in Table 2 and compared with the PES spectra in Figure 2. Qualitatively, the agreement between theory and experiment is quite good. The high density of valence states of $H_2P_2O_7^{2-}$ explains the congested PES spectra observed. Clearly, it was not feasible to have a one-to-one correspondence between the observed PES transitions and the valence MOs. The calculated orbital IPs are simply grouped according to the five spectral features in Table 2. The calculated IPs for the four deep valence MOs (12–15) are in the range of 4.96–6.19 eV, which were not observed even at 157 nm due to the cutoff by the RCB.

The valence MOs of $H_3P_3O_{10}^{2-}$ are also constructed from the oxygen lone-pair p orbitals. The calculated ADE and VDE for the ground-state transition of the global minimum of $H_3P_3O_{10}^{2-}$ (Figure 6a) is \sim 0.7 eV smaller than the experimental values (Table 1 and Figure 3). The ADEs calculated from the other two local minima (Figure 6b,c) are even smaller, and the VDEs are also smaller than the corresponding values from the global minimum structure. Because the two low-lying isomers are 7.8 and 11.9 kcal/mol higher in energy, they were probably not present in our experiment, consistent with the lack of any low binding energy features in the PES spectra (Figure 3). The calculated IPs are listed in Table 2 and shown in Figure 3. The calculated detachment energies, resulting from removing electrons from the first 17 occupied MOs are in qualitative agreement with the PES spectra, as indicated in Figure 3 and grouped in Table 2. The high density of valence states revealed in the calculation agrees well with the observed broad spectral features. Here again, detachment from the three deep MOs (15–17) was cut off by the RCB even at 157 nm (Figure 3c).

7. Conclusions

We report a combined photoelectron spectroscopic and computational study of $H_2PO_4^-$, $H_2P_2O_7^{2-}$, and $H_3P_3O_{10}^{2-}$. Global minima and low-lying isomers for the three anionic species were obtained. Detachment energies were also computed and compared to the experimental PES results. Five distinctive detachment features from $H_2PO_4^-$ were revealed and assigned to the top five occupied MOs, which are primarily oxygen lone-pair orbitals. The ADE and VDE of $H_2PO_4^-$ were measured to be 4.57 and 5.06 eV, respectively. We found that both $H_2P_2O_7^{2-}$ and $H_3P_3O_{10}^{2-}$ are stable in the gas phase with lower electron binding energies compared to $H_2PO_4^-$ due to their strong intramolecular Coulomb repulsion, which were estimated to be \sim 2.7 and \sim 2.3 eV, respectively. Only one structure was found for $H_2P_2O_7^{2-}$, whereas three stable conformations were identified for $H_3P_3O_{10}^{2-}$. All of the structures and isomers of the dianions contain intramolecular H-bonds. All of the valence MOs for the di- and triphosphate dianions also consist of oxygen lone pairs. The calculated detachment energies for $H_2P_2O_7^{2-}$ and $H_3P_3O_{10}^{2-}$ revealed a very high density of valence states

in both cases, consistent with the congested PES spectra observed. We also showed that higher multiply charged anions corresponding to the three phosphates with fewer protons than H_2PO_4^- , $\text{H}_2\text{P}_2\text{O}_7^{2-}$, and $\text{H}_3\text{P}_3\text{O}_{10}^{2-}$ are likely to be unstable in the gas phase due to the increased intramolecular Coulomb repulsion.

Acknowledgment. This work was supported by The U.S. Department of Energy, Office of Basic Energy Sciences, Chemical Science Division. The work was performed at the W. R. Wiley Environmental Molecular Sciences Laboratory, a national scientific user facility sponsored by DOE's Office of Biological and Environmental Research and located at Pacific Northwest National Laboratory, which is operated for DOE by Battelle.

References and Notes

- (1) Westheimer, F. H. *Chem. Rev.* **1981**, *81*, 313.
- (2) Westheimer, F. H. *Science* **1987**, *235*, 1173.
- (3) Ma, B.; Meredith, C.; Schaefer, H. F. *J. Phys. Chem.* **1994**, *98*, 8216.
- (4) Ma, B.; Meredith, C.; Schaefer, H. F. *J. Phys. Chem.* **1995**, *99*, 3815.
- (5) Colvin, M. E.; Eyleth, E.; Akacem, Y. *J. Am. Chem. Soc.* **1995**, *117*, 4357.
- (6) Saint-Martin, H.; Ruiz-Vicent, L. E.; Ramírez-Solís, A.; Ortega-Blake, I. *J. Am. Chem. Soc.* **1996**, *118*, 12167.
- (7) Blades, A. T.; Ho, Y.; Kebarle, P. *J. Phys. Chem.* **1996**, *100*, 2443; *J. Am. Chem. Soc.* **1996**, *118*, 196.
- (8) Wang, L. S.; Wang, X. B. *J. Phys. Chem. A* **2000**, *104*, 1978.
- (9) Wang, X. B.; Ding, C. F.; Wang, L. S. *Phys. Rev. Lett.* **1998**, *81*, 3551.
- (10) Wang, L. S.; Ding, C. F.; Wang, X. B.; Nicholas, J. B. *Phys. Rev. Lett.* **1998**, *81*, 2667.
- (11) Wang, X. B.; Wang, L. S. *Nature* **1999**, *400*, 245.
- (12) Wang, X. B.; Wang, L. S. *Chem. Phys. Lett.* **1999**, *313*, 179.
- (13) Wang, L. S.; Ding, C. F.; Wang, X. B.; Barlow, S. E. *Rev. Sci. Instrum.* **1999**, *70*, 1957.
- (14) High Performance Computational Chemistry Group. NWChem, A Computational Chemistry Package for Parallel Computers, Version 4.0.1. Pacific Northwest National Laboratory, Richland, WA 99352, 2001.
- (15) Andzelm, J. In *Density Functional Methods in Chemistry*; Labanowski, J., Andzelm, J., Eds.; Springer-Verlag: New York, 1991; p 155.
- (16) Ziegler, T. *Chem. Rev.* **1991**, *91*, 651.
- (17) Becke, A. D. *J. Chem. Phys.* **1993**, *98*, 5648.
- (18) Lee, C.; Yang, W.; Parr, R. G. *Phys. Rev. B* **1988**, *37*, 785.
- (19) Godbout, N.; Salahub, D. R.; Andzelm, J.; Wimmer, E. *Can. J. Chem.* **1992**, *70*, 560.
- (20) Dunning, T. H.; Hay, P. J. In *Modern Theoretical Chemistry*; Schaefer, H. F., Ed.; Plenum Press: New York, 1977; Vol. 2.
- (21) Black, G.; Chase, J.; Didier, B.; Feller, D.; Gracio, D.; Jones, D.; Keller, T.; Matsumoto, S.; Mendoza, E.; Olander, M.; Palmer, B.; Peden, N.; Schhardt, K.; Taylor, H.; Thomas, G.; Vorpagel, E.; Windus, T. Ecce, A Problem Solving Environment for Computational Software, Version 1.5. Pacific Northwest National Laboratory, Richland, WA 99352, 1999.
- (22) Kim, H. S.; Yu, M.; Jiang, Q.; LeBreton, P. R.; *J. Am. Chem. Soc.* **1993**, *115*, 6169.
- (23) Wang, X. B.; Wang, L. S. *Phys. Rev. Lett.* **1999**, *83*, 3402.
- (24) Wang, X. B.; Ding, C. F.; Wang, L. S. *Chem. Phys. Lett.* **1999**, *307*, 391.
- (25) Fetzer, S. M.; LeBreton, P. R.; Rohmer, M.-M.; Veillard, A. *Int. J. Quantum Chem.* **1997**, *65*, 1095.